Indonesian Physical Review
Volume 07 Issue 03, September 2024
P-ISSN: 2615-1278, E-ISSN: 2614-7904

Synthesis and Characterization of Magnetite Nanomaterials in Tianyar Iron Sand Using Co-precipitation Method

Ni Putu Devi Kristina[1*], I Gede Arjana[2*], Putu Yasa[3*]
[1] *Physics and Science Teaching Department, Faculty of Mathematics and Natural Science, Ganesha University of Education, Indonesia*

Corresponding Authors E-mail: devi.kristina@undiksha.ac.id, igede.arjana@undiksha.ac.id, pt.yasa@undiksha.ac.id

Article Info

Article info:
Received: 21-03-2024
Revised: 20-07-2024
Accepted: 24-07-2024

Keywords:
Coprecipitation method; Irond sand; Magnetite (Fe_3O_4) nanomaterials; SEM-EDS; X-Ray Diffraction (XRD)

How To Cite:
N. P. D. Kristina, I. G. Arjana, and P. Yasa, "Synthesis and Characterization of Magnetite Nanomaterials in Tianyar Iron Sand Using Co-precipitation Method", Indonesian Physical Review, vol. 7, no. 3, p 398-413, 2024.

DOI:
https://doi.org/10.29303/ipr.v7i3.328.

Abstract

In the current era of scientific and technological progress, nanomaterials have emerged as a deeply fascinating and significant field of research. This paper presents a case study on the synthesis and characterization of Fe_3O_4 nanomaterials derived from the iron sand of the Tianyar, utilizing the co-precipitation method with modifications made to the pH values during synthesis. The research encompasses three primary stages: extraction of iron sand, synthesis of Fe_3O_4 nanomaterials, and subsequent characterization of these nanomaterials. The iron sand extraction phase involved passing it through a permanent magnet ten times to remove impurities. Subsequent synthesis produced a dark black magnetite nanomaterial powder displaying magnetic properties, rendering it responsive to magnet attraction. Analysis of these nanomaterials using X-ray diffraction (XRD) unveiled discernible peaks in the diffraction pattern, suggesting that the magnetite nanomaterials possess a cubic crystal structure. The size of the Fe_3O_4 nanomaterials decreases as the pH of precipitation increases, with respective sizes of approximately 18.00 nm for pH 9, 14.69 nm for pH 10, and around 13.68 nm for pH 11, as determined using Scherrer's formula. The lattice parameters observed for samples synthesized at pH 9, 10, and 11 are sequentially measured as a = 8.59 Å, 8.81 Å, and 8.80 Å. Analysis using SEM-EDS revealed that the sample morphology appears rough, with evidence of particle agglomeration leading to uneven particle distribution. There are additional trace elements present, including C, Al, S, Ti, and Cl, albeit in smaller quantities. Nevertheless, the primary elements crucial for forming Fe_3O_4 nanomaterials, namely Fe and O, exhibit the highest percentages in composition analysis.

Introduction

In the contemporary age of scientific and technological advancements, nanomaterials have surfaced as a profoundly captivating and important area of study. Nanomaterials are substances characterized by their dimensions falling within the range of 1 to 100 nanometers, where their nanoscale size results in at least one distinctive property differing significantly from its larger-scale counterpart [1]. At the nanometer scale, materials exhibit distinct physical,

chemical, and biological properties compared to their bulk counterparts. Materials engineered at the nanoscale demonstrate heightened performance sensitivity compared to those at larger scales. This heightened sensitivity primarily stems from nanomaterials' larger specific surface area, which amplifies their reactivity levels [2]. Nanomaterials can be categorized into five groups based on factors like size, origin, structural arrangement, pore size, and potential toxicity. In particular, inorganic nanomaterials are typically classified as either metal-based or metal oxide-based. Metal-oxide nanomaterials are distinguished by their composition, comprising negative oxygen ions and positive metallic ions [3]. In comparison to other metal oxide nanomaterials, iron oxides exhibit notable characteristics such as high adsorption capacity, surface reactivity, magnetic properties, and catalytic efficiency. These attributes are attributed to their biocompatibility, superparamagnetism, and ultrafine size [4].

Magnetite (Fe_3O_4) belongs to the iron oxide mineral group and is well-known for its cubic crystal structure and remarkably robust magnetic properties [5]. In recent times, magnetite nanomaterials (Fe_3O_4) have found diverse applications, including biosensing for diagnostic purposes , drug delivery [7], and hyperthermia therapy [8]. Iron oxide exists in various natural forms. Among them, iron oxide can be readily found in iron sand [9]. Iron sand is essentially black and dark ash in color [10]. One of the areas abundant in iron sand is situated in Tianyar Village, Bali. The presence of iron sand in this region is influenced by the activity of nearby volcanoes, particularly Mount Agung. The volcanic activity results in the deposition of lava and ash, forming cliffs or moving downslope, ultimately serving as a source of sediment. During the wet season, rivers transport this sediment into the sea, contributing to the accumulation of iron sand in the area [11]. According to the findings of the heavy mineral analysis, the study area contains a variety of mineral groups, including oxides, hydroxides, silicates, sulfides, carbonates, and mica groups [12].

In 2021, the Karangasem district witnessed significant growth in mining and excavation activities, particularly in the extraction of sand and rocks. However, the primary concern for this sector revolves around the environmental degradation resulting from these excavations [13]. Converting iron sand into magnetic material can greatly increase its commercial value. One effective strategy to achieve this is by utilizing iron sand as a fundamental ingredient in the production of magnetite (Fe_3O_4) nanomaterials. Several synthesis methods exist for producing Fe_3O_4 nanomaterials, among which co-precipitation is a commonly employed technique [14], Chemical Vapor Deposition (CVD) [15], Sol-Gel [16], ball milling [17], and thermal decomposition [18]. The objective of these synthetic processes is to modify the properties and size of the magnetite particles or crystals produced [19]. The co-precipitation method stands out as the simplest synthesis process for producing Fe_3O_4, involving minimal steps and low temperatures (below 100°C). Magnetite nanomaterials are achieved through the co-precipitation of ferrous and ferric salts in an aqueous solution with varying Fe^{3+}/Fe^{2+} ratios, employing a strong ammonia-based basic solution at room temperature or higher. This approach offers a straightforward and cost-effective means of generating Fe_3O_4 powder from raw iron sand materials [20].

Co-precipitation synthesis often involves variations in pH, molar ratio [21], reaction temperature [22], and stirring rate [23]. Changes in pH levels can influence the chemical state of a solution, affecting reaction kinetics and particle sedimentation. This variation can lead to several consequences: 1) Particle size, where different pH values can regulate nucleation and particle growth rates, resulting in particles of varying sizes; 2) Morphology, as pH can alter particle shapes, causing them to become rounded or stem-shaped due to its impact on crystal

growth; 3) Crystal structure, where pH may influence the formation of specific crystal phases and the distribution of crystals within the material [24]. Despite extensive research on Fe_3O_4 synthesis, there is a gap in understanding the precise effects of pH variations on the resulting nanomaterials, particularly those derived from natural iron sand. This study aims to fill that gap by systematically exploring how pH control during synthesis affects the physical and chemical properties of Fe_3O_4 nanoparticles.

In the investigation of Fe_3O_4 nanomaterials, characterization was conducted through XRD (X-ray diffraction) and SEM-EDS (Scanning Electron Microscopy-Energy Dispersive X-ray Spectroscopy) techniques. XRD analysis is utilized to determine crystal lattice parameters, crystal structure, and particle size. On the other hand, SEM-EDS is employed to produce microscopic surface images and analyze the elemental composition of the material, facilitating exploration of its structure and composition. The objective of this study is to synthesize and characterize Fe_3O_4 nanomaterials derived from iron sand using the co-precipitation method with variations in pH control. This research is important as it seeks to enhance the practical use-value of natural iron sand, contributing to the development of advanced magnetic materials with specific properties tailored through precise pH adjustments during synthesis.

Theory and Calculation

Bragg's Law and Scherrer's Formula

X-ray diffraction (XRD) is a powerful analytical method used to study atomic and molecular arrangements in materials. It helps determine properties like crystal structure, lattice dimensions, phase composition, and crystallite dimensions [25]. The process occurs due to constructive interference between waves scattered from lattice planes and diffracted by the crystalline sample, following Bragg's law.

$$\lambda = 2d \sin \theta \quad (1)$$

Here, d represents the interplanar distance, and λ stands for the wavelength of the X-rays. The intensity of the diffracted beam is recorded concerning the diffraction angle 2θ and the orientation of the specimen. Smaller crystals may display observable signals near the Bragg angle, resulting in peak broadening. Investigating X-ray scattering at angles deviating from the Bragg angle is valuable for estimating the size of small crystals [26]. Factors contributing to diffraction peak broadening include incident beam non-parallelity and the characteristic line used.

As the size of crystals decreases, the size effect becomes increasingly significant relative to other factors, rendering the Scherrer formula applicable. This formula correlates the size of sub-micrometer particles or crystallites in a solid with the broadening of a diffraction peak and is commonly employed for determining the size of crystalline particles, particularly in powder form. The average crystallite size (D) is calculated from the full-width half maximum (FWHM) of the peaks in radians [27].

$$D = \frac{k\lambda}{B \cos \theta} \quad (2)$$

For magnetite nanomaterials, k = 0.94, λ is the wavelength of XRD, and θ is the diffraction angle.

Experimental Method

This study adopts an experimental research approach, wherein one or more independent variables are manipulated to observe their effects on one or more dependent variables. In this research, the independent variables include the pH of the solution, specifically at levels of 9, 10, and 11, determined using 25% NH_4OH. These variables are anticipated to influence the dependent variables, which encompass crystal structure, crystal size, and crystal morphology. Experiments were conducted to analyze the characteristics of Fe_3O_4 nanomaterial synthesis derived from iron sand extraction through the co-precipitation method with pH variation. Subsequently, the synthesized materials were characterized using X-ray powder diffractometer (Rigaku SmartLab X-ray diffractometer, Tokyo, Japan) and SEM-EDS (JSM 5510, JEOL, Tokyo, Japan) techniques to ascertain crystal structure, lattice parameters, and crystal size.

Iron sand samples were collected from Tianyar Village, Karangasem District, Bali Province. The extraction process, Fe_3O_4 synthesis via co-precipitation methods, and characterization of magnetic Fe_3O_4 were carried out at the Laboratory of the Department of Materials Engineering, Ming Chi University of Technology, Taiwan. The materials used for synthesis included 6.27 grams of pure iron sand, 30 mL of 37% HCL obtained from Scharlau, Scharlab, Barcelona, Spain, 8.96 grams of $FeSO_4$ purchased from Acros, and 80 mL of NH_4OH (Ammonium Hydroxide) acquired from Riedel-deHaen. This research is carried out in three stages, namely: (1) Stage of extraction of Tianyar iron sand degree, (2) Stage of Magnetic mineral synthesis Fe_3O_4, and (3) Stage Characterization of mineral synthetic magnetite Fe_3O_4.

1. Extraction of Tianyar Iron Sand
   The extraction stage of iron sand was carried out using a permanent magnet. The extraction of iron sand utilizes the magnetic properties of the magnetite mineral, allowing it to separate from impurities. Extraction is performed to obtain purer magnetite and is repeated 10 times.
2. Synthesis of Fe_3O_4 Using the Co-Precipitation Method
   The synthesis of Fe_3O_4 begins by weighing approximately 6. 27 grams of iron sand. Next, a solution of 37% HCl is poured into a measuring cylinder, totaling 30 ml. These two substances are then mixed in a beaker, and stirred using a magnetic stirrer on a hot plate for 1 hour at a temperature of 55°C and a rotational speed of 600 rpm. Afterward, the solution is filtered twice using filter paper. Then, $FeSO_4$ powder (99%) as much as 8. 96 was dissolved with 15 ml of distilled water to become FeSO4 solution. These two solutions, namely FeCl3 and FeSO4 solutions, were mixed in a breaker and then stirred with a magnetite stirrer for 15 minutes. After that, 5 ml of the solution was titrated by adding 25 % ammonia (NH_4OH) while being stirred by a magnetic stirrer on a hot plate at a temperature of 55 °C to achieve the desired pH levels of 9, 10, and 11.
   After reaching the desired pH, the solution is left on the hot plate and stirred for 1 hour until the solution becomes black in color. Subsequently, the co-precipitation process solution is washed several times with deionized water to remove the base (neutral pH), and the precipitate is dried on a hot plate at a temperature of 60 °C until it becomes a dry powder. The chemical reaction equation leading to the formation of the Fe_3O_4 precipitate can be seen in Reaction (1) below.

$$FeSO_4 + 2FeCl_3 + 8\ NH_4OH \rightarrow Fe_3O_4 + (NH_4)2\ SO_4 + 6NHCl\ 4H_2O \quad (1)$$

The Fe_3O_4 powder produced is then stored in small airtight glass bottles for subsequent characterization.

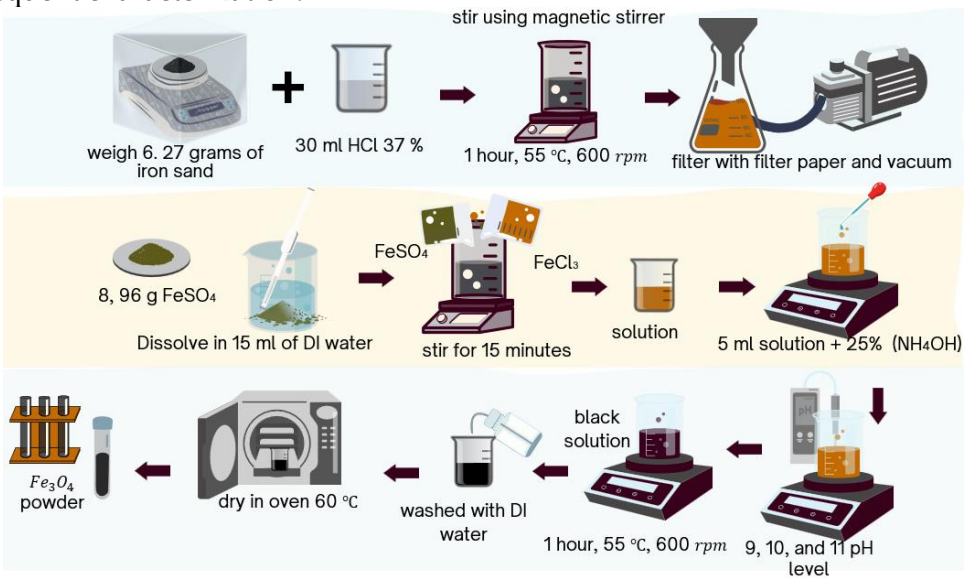

Figure 1. Synthesis process of Fe_3O_4 nanomaterials

3. Sample Characterization
   a. X-ray Diffractometer (XRD)
      X-ray diffractometer (XRD) is a common technique used to determine the crystallographic characteristics of a material through the appearance of intensity peaks. The XRD instrument used in this final project research is the Philips X'Pert MPD (Multi-Purpose Diffractometer) located in the Laboratory of the Department of Materials Engineering at Ming Chi University of Technology, Taiwan. Sample testing was conducted within the 2θ angle range of $15° \; to \; 80°$ using Cu as the X-ray source ($\lambda = 1.5406$ Å). The XRD data obtained were then qualitatively phase-identified using the Origin software. Meanwhile, crystal size was quantitatively analyzed using Scherrer's formula.
   b. Morphological Test with SEM-EDS
      Testing utilizing Scanning Electron Microscopy (SEM) is conducted to gain a comprehensive morphological overview of the samples under examination. Additionally, Energy Dispersive X-ray Spectroscopy (EDS) testing is employed to qualitatively determine the elemental composition in specific areas of the material and can generate distribution mappings of its elements. Following heat treatment, samples are analyzed, and the atom percentage before treatment is compared with the results. Morphological surface images obtained through SEM reveal details such as crystal grain size, distribution, and porosity of each sample. Concurrently, composition analysis of the sample surface is obtained quantitatively. Data acquired from SEM-EDS characterization are presented in the form of photographs captured at various magnifications, including 500x, 1,000x, 3,000x, 5,000x, and 10,000x, facilitating a detailed examination of the samples at different scales. Thus, from these

surface morphological images, an analysis of the distribution composition of magnetite Fe_3O_4 is obtained.

Result and Discussion

1. Synthetic Results of Nanomaterials Magnetite (Fe_3O_4)

Tianyar iron sand has successfully synthesized Magnetite (Fe_3O_4) nanomaterial compounds using co-precipitation methods with variations in pH value. During the dissolution stage, iron sand extract undergoes solubilization, resulting in a concentrated, black-shaped solution indicative of the iron salt content. Iron sand extracts are dissolved using a high concentration of HCl solution, as the iron metal present in the iron sand extract readily reacts with HCl to form iron (II) chloride (Figure 2 a). The resulting solution of iron salt is subsequently introduced by means of an NH_4OH solution injection. The precipitation of iron salt deposits may arise from the formation of mixed crystals or from ion-ion adsorption during the sedimentation phase. These deposits emerge because of the oxidation process involving the iron metal content within the solvent's iron salts (Figure 2 b).

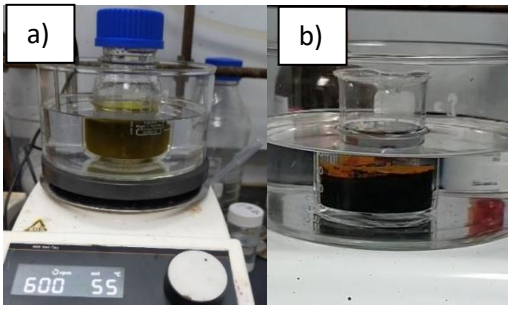

Figure 2. Synthesized findings encompass (a) the dissolution phase and (b) the sedimentation phase.

Figure 3 shows differences in iron sand extract before and after synthesis with co-precipitation methods. Based on direct observations, there is a noticeable distinction between the iron sand extract and the synthesized results. The synthetic magnetite minerals appear to possess a darker concentration compared to the iron sand extracts.

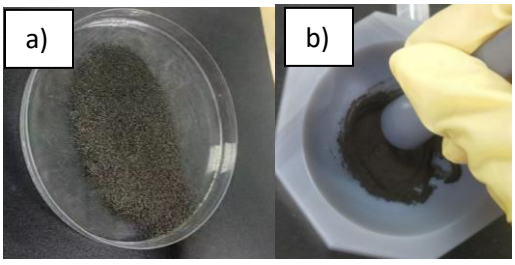

Figure 3. Synthesized magnetite nanomaterials results comprise (a) iron sand extraction prior to synthesis and (b) iron sand extraction subsequent to synthesis.

2. Characterization Results Using XRD

Using the ORIGIN software, crystal structure analysis can be performed by matching the diffracted peak with the base data from JCPDS No. 65-3107. The peak signifies the

correspondence of order between the wavelength and the width of the magnetite material lattice. These enhancements elucidate the nature of the magnetite material formed synthetically. It is known that the angle at the top of the diffraction can be used to calculate the width of the crystallites in the synthetic magnetite material according to the Schrerrer's Formula. The XRD pattern from the fractioned peak showed similarities with the magnetite peak in the database. This suggests that the material formed by the synthesis is a magnetite material. Based on this analysis, information about the structure of magnetite crystals can be obtained. Figure 4 shows that the diffracted peaks in the three Fe_3O_4 samples after synthesis experience proliferation and increased intensity as the pH variation is increased. This indicates that the higher the pH of the sample, the smaller the crystal (Tabel 1).

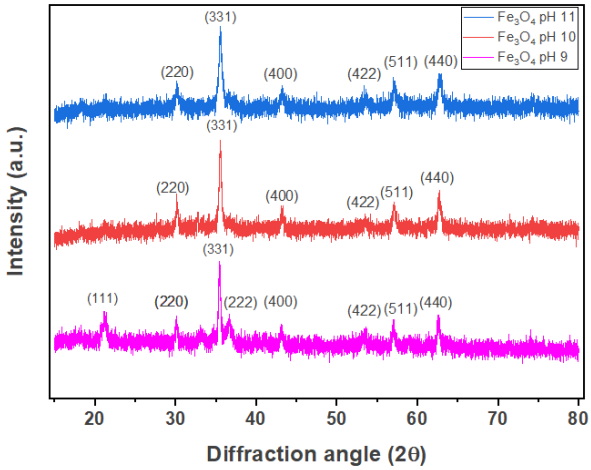

Figure 4. XRD patterns of the product synthesized (Fe_3O_4) from three samples.

Based on the diffraction graph pattern above, information is obtained regarding the interpretation of the resulting diffraction peaks. The calculation of crystal size using the Debye-Scherrer equation.

Table 1. Calculation of crystal size in pH variations

pH 9			pH 10			pH 11		
2θ	**FWHM**	**Crystal size (nm)**	**2θ**	**FWHM**	**Crystal size (nm)**	**2θ**	**FWHM**	**Crystal size (nm)**
21.17	1.29	6.28	30.18	0.35	22.20	30.20	0.52	15.68
30.10	0.39	21.16	35.55	0.41	18.64	35.57	0.56	15.01
35.47	0.34	24.40	43.21	0.44	16.73	43.23	0.54	15.87
36.58	1.03	8.08	53.53	1.51	4.71	53.63	0.93	9.60
43.13	0.36	23.64	57.14	0.53	13.07	57.16	0.67	13.58
53.38	0.63	14.11	62.73	0.53	12.79	62.79	0.75	12.38
57.04	0.41	21.88						
62.62	0.38	24.44						
Average crystal size		**18.00**			**14.69**			**13.68**

3. Characterization Results Using SEM

The morphological structure of Fe_3O_4 using SEM can be shown in figure 5 to figure 9. That represent the morphologic structure of Fe_3O_4, with magnifications of 500 x, 1000 x, 3000 x, 5000 x, and 10,000 x. It appears that Fe_3O_4 particles tend to accumulate to form clumps. The above picture shows that the surface of the accumulated particles varies in degree. The SEM imaging results showed the morphological shape of a round and cube-shaped Fe_3O_4 nanomaterials with porous cavities.

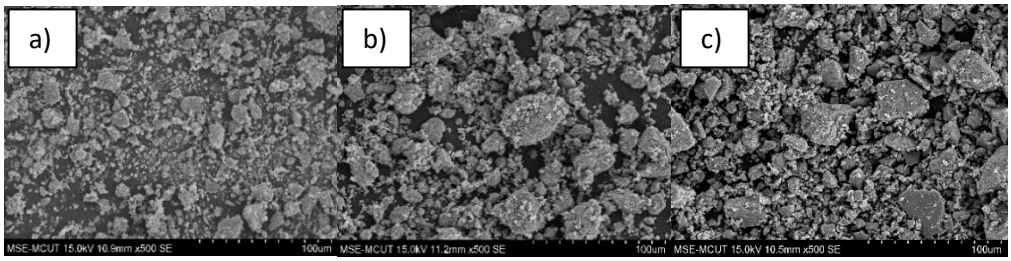

Figure 5. The morphological structure of Fe_3O_4 observed through SEM at 500x magnification, under varying pH conditions: (a) pH 9, (b) pH 10, and (c) pH 11.

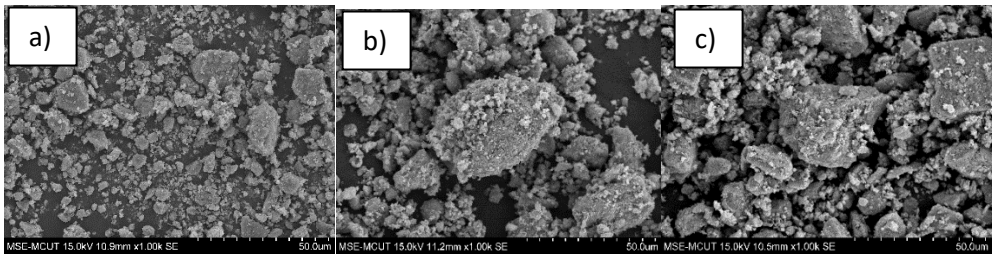

Figure 6. The morphological structure of Fe_3O_4 observed through SEM at 1000 x magnification, under varying pH conditions: (a) pH 9, (b) pH 10, and (c) pH 11

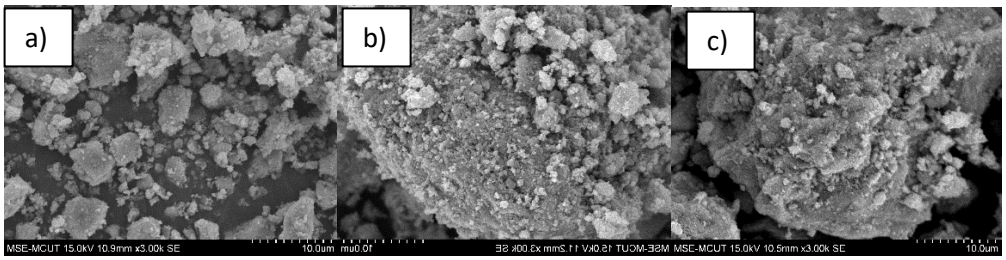

Figure 7. The morphological structure of Fe_3O_4 observed through SEM at 3000 x magnification, under varying pH conditions: (a) pH 9, (b) pH 10, and (c) pH 11

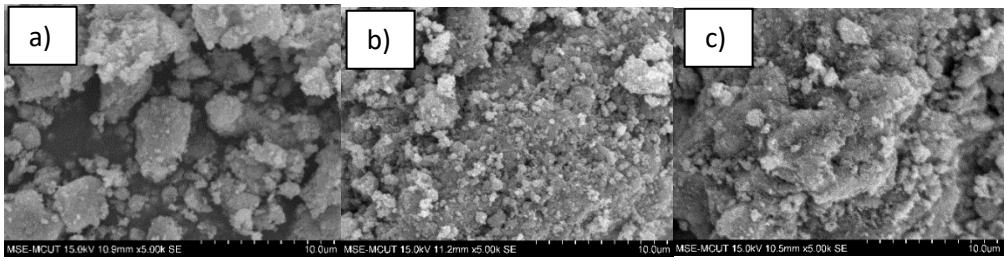

Figure 8. The morphological structure of Fe_3O_4 observed through SEM at 5000 x magnification, under varying pH conditions: (a) pH 9, (b) pH 10, and (c) pH 11

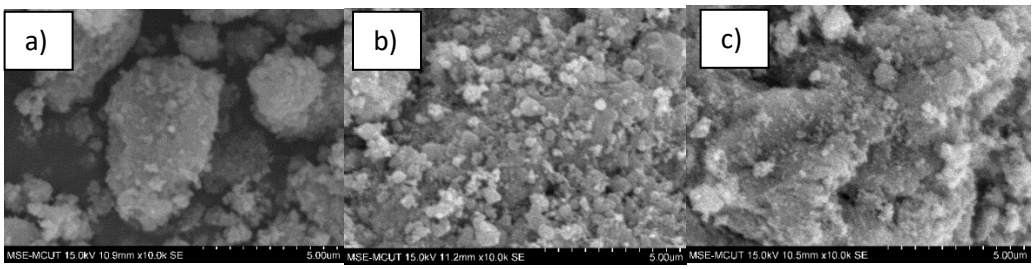

Figure 9. The morphological structure of Fe_3O_4 observed through SEM at 10,000 x magnification, under varying pH conditions: (a) pH 9, (b) pH 10, and (c) pH 11

4. Characterization Results Using EDS

Further, the results of the elements or content of the sample after synthesis can be determined from the EDS results. Figure 10 shows the elements found in varying pH value that have been synthesized with pH 9 as more details can be seen in Table 2.

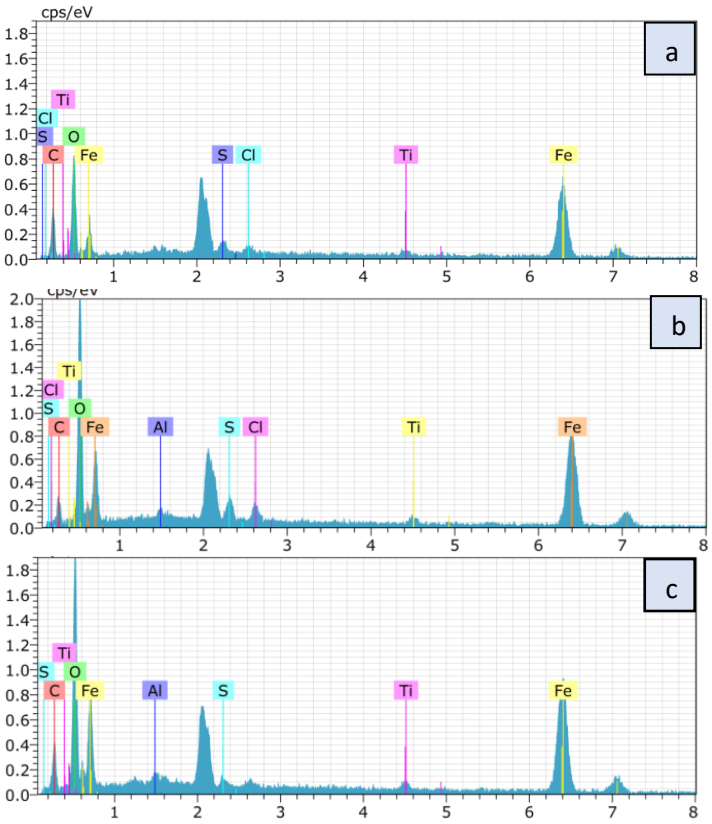

Figure 10. The elements detected via EDS in varying pH conditions: (a) pH 9, (b) pH 10, and (c) pH 11.

Table 2. The elemental composition percentages identified through EDS were synthesized at pH 9, 10, and 11.

pH 9		pH 10		pH 11	
Element	Mass (%)	Element	Mass (%)	Element	Mass (%)
C	15. 16	C	6. 43	C	8. 95
O	17. 54	O	25. 78	O	15. 80
S	2. 44	Al	0. 66	Al	0. 67
Cl	1. 73	S	1. 55	S	0. 13
Ti	1. 99	Cl	1. 17	Ti	0. 97
Fe	61. 13	Ti	1. 32	Fe	65. 54
		Fe	63. 08		
Total mass (%)					**100. 00**

In the pH 9 specimen, the highest mass content of elements are Fe at 61.13% and O at 17.54%. Additionally, coagulant elements formed during synthesis include C (15.16%), S (2.44%), Ti (1.99%), and Cl (1.73%). For the pH 10 specimen, Fe is the highest at 63.08%, followed by O at 25.78%. Coagulant elements present are C (6.43%), S (1.55%), Ti (1.32%), Cl (1.17%), and Al (0.66%). In the pH 11 specimen, Fe content is highest at 65.54%, and O is 15.80%. Other coagulant elements include C (8.95%), S (0.13%), Ti (0.97%), and Al (0.67%).

Discussion

1. Synthetic

Based on the analysis of the three Fe_3O_4 nanomaterial synthesis results, it was found that the three samples had identical colours, i.e. concentrated black. Magnetite has a black pigment, so it is known as black iron oxide, while iron like hematite and maghemite have other characteristics: red and brown [28]. From the results of this research the powder was produced is a concentrated black powder that marks the characteristic characteristics of the magnetite (Fe_3O_4) nanoparticles.

$FeCl_3$ is used as a source of Fe^{3+} ions and $FeSO_4$ solution as a Fe^{2+} ion source because ferrous and ferric ions are the basis of the Fe_3O_4 nanoparticles synthesis. The formation of nanoparticles by co-precipitation of the solution is done by sedimentation with NH_4OH which provides a base atmosphere in the solution system. A black precipitate will form as soon as the solution of the first reaction is mixed with the base solution. This rapid reaction of formation is the cause of a nanosized Fe_3O_4 particle. The resulting iron oxide deposits are concentrated in black, indicating the formation of Fe_3O_4. [29]. In addition to black, the three samples formed are also magnetite particles that have been shown to interact with the magnetic field.

2. XRD Characterization

On the XRD, the width of the diffraction peak can provide information about the size of the crystal. The smaller the crystal size, the larger the diffraction of the fragmented peak. This is known as peak expansion due to the wider crystal size distribution. Increases in diffraction peak intensity can occur due to increased number and diversity of smaller crystal sizes. The

size of the crystals in this study was influenced by the changes in the pH used in the synthesis process. At a higher pH, this process can be more controlled, producing smaller particles due to more crystal core formation and more limited crystal growth [30]. Therefore, the Fe_3O_4 pH 11 sample has a smaller particle size than the other sample.

Increased pH levels during Fe_3O_4 synthesis can significantly influence the nucleation and crystal growth processes. This phenomenon often leads to a decrease in particle size as the pH of the solution rises. The mechanism behind this phenomenon involves the interplay of interfacial tension and ionic forces during the dissolution and recrystallization processes, ultimately resulting in either increased particle growth or a specific reduction in surface area [31]. The surplus of ions present in the solution leads to a decrease in interfacial voltage, slowing down the particle growth rate. As a result, the overall particle size tends to decrease, or the surface area becomes more specifically reduced as pH levels increase during synthesis [24].

During the preparation phase, it is crucial to regulate the size of nanoparticles to ensure their suitability for applications such as drug delivery and hyperthermia treatment in cancer therapy. Nanoparticles ranging from 10 to 100 nm are considered optimal for these purposes. All three samples examined in this research yielded magnetite nanomaterials within this size range, indicating their potential utility in biomedical applications. Their extended flow duration within the body is attributed to their ability to bypass the reticuloendothelial system and access small vessels. In the case of magnetic nanoparticles, smaller sizes enhance their penetration and retention effects, leading to maximum nanoparticle accumulation at the intended site [32].

3. SEM Characterization

Analysis using SEM aims to determine surface morphology on nanomaterials Fe_3O_4. Based on the analysis of the three samples using SEM with magnifications of 500 times, 1000 times, 3000 times, 5000 times, and 10,000 times, the particle details on the iron sand sample have an irregular and rough shape. This can be stated from previous research, in which the obtained magnetite structure is irregular and tends to form aggregates [33]. The SEM test also revealed particles that cling to each other, resulting in agglomeration. This agglomeration occurs due to the instability of the particles in the solution during the synthesis process so that in order to stability, these particles will try to bind to each other [34].

This study found that increased pH can affect particle agglomeration. Some factors that can explain the relationship between high pH and agglomeration involve changes in particle surface properties and equilibrium between interparticle styles. At a high pH, changes in ion balance in the solution can affect the co-precipitation and particle formation processes. More hydroxide ions can interact with iron ions, alter the solution balance, and ultimately affect the agglomeration. Increased pH can cause an increase in hydroxide (OH-) ions in the solution. If Fe_3O_4 particles have a negative surface load, an increase in hydroxide ions can reduce the negative surface charge. This can reduce torque between particles, which can increase the agglomeration [35].

Furthermore, the sample exhibits a non-uniform particle size distribution, as evidenced by the particle distribution results. These findings indicate that higher pH levels used in the synthesis process led to greater variability in the sizes of the formed crystals. The influence of increased pH on reaction speed and particle formation mechanisms can significantly impact the time required for crystal formation and the types of phases formed. If phase formation is not uniform, it can adversely affect the uniformity of crystal sizes [36].

4. EDS Characterization

Based on the results of the analysis, the three samples of the synthetic results contained the iron and oxygen elements that form the Fe_3O_4 nanomaterial of Tianyar iron sand as the base material, as well as containing several other corrosives, such as carbon, sulphur, titanium, aluminium, and chloride. In the process of Fe_3O_4 synthesis using co-precipitation methods, pH adjustment can affect the iron content produced. The iron element (Fe) is the main component in the synthesis of Fe_3O_4 as a precursor and this process is designed to create simultaneous precipitates of the iron compound with other compounds. At a higher pH, hydroxide (OH^-) ions will be more present in the solution. Hydroxide ions can react with iron ions (Fe^{2+}) and (Fe^{3+}) to form less soluble iron hydroxide compounds. This process allows for the formation of more efficient iron precipitates, which can ultimately produce a higher iron content in the final product [37].

The presence of oxygen (O) is a crucial component of the structure of the synthesized compound Fe_3O_4. In the synthesis reaction, oxygen derived from water molecules (H_2O) actively contributes to the formation of the Fe_3O_4 structure by facilitating oxide bonds between iron atoms. As such, the presence of oxygen elements in the synthesis of Fe_3O_4 via the co-precipitation method is inherent to the oxide compound's structure. Consequently, iron and oxygen are not considered contaminants or additional elements but are fundamental constituents of the magnetite nanomaterial produced. However, it's essential to recognize that excessively high pH regulation may influence the formation of other compounds or induce unfavourable conditions. Therefore, pH regulation must be optimized to ensure that reaction conditions are conducive to the optimal formation of Fe_3O_4. This optimization is critical to guaranteeing the desired characteristics and properties of the synthesized nanomaterial.

In the three samples also found the carbon element (C) with the highest presentation. The presence of carbon elements in the final product may be derived from a certain source or factor during the synthesis process. Carbon is assumed to be black carbon, derived from a sample that cannot be dissolved during the washing process and does not evaporate during the calcination process [38]. In addition, during the synthesis process iron particles can capture carbon from the air, especially if the experimental conditions are not carried out in an entirely carbon-free environment or if laboratory settings are inadequate.

In addition, titanium and sulphur were found in each of the three samples. In synthesis with pH 9 and 10 chloride was found, but pH 11 was not found. Then in pH 10 and 11 aluminium was found but in pH 9 was not. The presence of titanium (Ti) and aluminium (Al) elements in Fe_3O_4 synthesis products by co-precipitation methods may be caused by certain factors and conditions during the synthesisation process. [39]. The presence of the chloride element (Cl) in

the Fe_3O_4 synthesis by the co-precipitation method is due to the use of chloride compounds as a precursor or solution of the reagent during the synthesisation process. In some synthetic protocols, a hydrochloric acid solution (HCl) was used as a reagent to influence reaction conditions or accelerate sedimentation. The use of HCl can cause the chloride element to enter the final product. The presence of the sulphur element (S) in the Fe_3O_4 synthesis by the co-precipitation method is influenced by the additive raw material or additive agent used in the synthesis, namely iron sulphate ($FeSO_4$), which contains sulphur compounds that can enter the final product.

Conclusion

Magnetite (Fe_3O_4) nanomaterials were successfully synthesized using co-precipitation method with pH variations (9, 10, 11) based on Tianyar iron sand so that they formed a powder of Fe_3O_4 nanomaterials that is black and can be attracted by magnets on the three samples. The characteristics of the Fe_3O_4 nanomaterials from the synthesized sample can be demonstrated from both XRD and SEM-EDS results. The parameters of the mesh and the particle size produced on the sample with pH 9, 10, and 11 in succession are a = 8, 59 Å with 18, 00 nm; a = 8, 81 Å with 14, 69 nm; a= 8, 80 Å with 13, 68 nm. It appears that the higher the pH used, the smaller the particle size produced. According to SEM-EDS characterization results, the sample displays a rough morphology with particle agglomeration, resulting in uneven particle distribution. However, the elemental composition analysis reveals that iron (Fe) and oxygen (O), the primary elements in Fe_3O_4 nanomaterial formation, constitute the highest percentage, alongside trace elements including carbon (C), aluminum (Al), sulfur (S), titanium (Ti), and chlorine (Cl).

Acknowledgment

The finalization of this manuscript would not have been possible without the assistance of numerous individuals. Hence, the author would like to extend sincere gratitude to all those who contributed their support and assistance throughout this endeavor.

1. Professor Ting-Yu Liu provided guidance and resources for conducting research at Ming Chi University of Technology, Taiwan.
2. Dr. Kuan-Syun Wang and Dr. Yun-Chu Chen, serving as Assistant Research, offer direction and guidance for research activities at the Ming Chi University of Technology, Taiwan.
3. The faculty members of the Physics Education Department have generously shared their knowledge, insights, and guidance throughout the entirety of this research, from its inception to the culmination of its results.

References

[1] C. M. Donegá, *Nanoparticles Workhorses of Nanoscience*. 2014.
[2] J. Jeevanandam, A. Barhoum, Y. S. Chan, A. Dufresne, and M. K. Danquah, "Review on nanoparticles and nanostructured materials: history, sources, toxicity and regulations," *Beilstein J Nanotechnol,* vol. 9, pp. 1050-1074, 2018, doi: 10.3762/bjnano.9.98.
[3] B. Mekuye and B. Abera, "Nanomaterials: An overview of synthesis, classification, characterization, and applications," *Nano Select,* vol. 4, no. 8, pp. 486-501, 2023, doi: 10.1002/nano.202300038.

[4] R. Revathy, T. Sajini, C. Augustine, and N. Joseph, "Iron-based magnetic nanomaterials: Sustainable approaches of synthesis and applications," *Results in Engineering,* vol. 18, 2023, doi: 10.1016/j.rineng.2023.101114.
[5] I. Khan, K. Saeed, and I. Khan, "Nanoparticles: Properties, applications and toxicities," *Arabian Journal of Chemistry,* vol. 12, no. 7, pp. 908-931, 2019, doi: 10.1016/j.arabjc.2017.05.011.
[6] S. L.-S. Carinelli, Maximina González-Mora, José Luis Salazar-Carballo, Pedro Ángel, "Synthesis and Modification of Magnetic Nanoparticles for Biosensing and Bioassay Applications: A Review," Creative Commons CC, 2023, doi: 10.20944/preprints202307.1398.v1. Creative Commons CC BY.
[7] L. Shen, B. Li, and Y. Qiao, "Fe(3)O(4) Nanoparticles in Targeted Drug/Gene Delivery Systems," *Materials (Basel),* vol. 11, no. 2, Feb 23 2018, doi: 10.3390/ma11020324.
[8] A. Wlodarczyk, S. Gorgon, A. Radon, and K. Bajdak-Rusinek, "Magnetite Nanoparticles in Magnetic Hyperthermia and Cancer Therapies: Challenges and Perspectives," *Nanomaterials (Basel),* vol. 12, no. 11, May 25 2022, doi: 10.3390/nano12111807.
[9] Y. G. W. I Safitri, D Rosarina and Sudibyo, "Synthesis and characterization of magnetite (Fe3 O4) nanoparticles from iron sand in Batanghari beach," IOP Conf. Ser.: Mater. Sci. Eng., 2020, doi: 10.1088/1757-899X/1011/1/012020.
[10] S. Aritonang, Jupriyanto, Juhana, R., "Analysis of The Process of Iron Sand Processing Into Sponge Iron in Order to Support The Defense Industry Of Steel Raw Materials," *Jurnal Pertahanan & Bela Negara,* vol. 9, 1, 2019.
[11] H. Kurnio, "Coastal characteristics of iron sand deposits in Indonesia," *Indonesian Mining Journal,* vol. 10, p. 27, 2019.
[12] I. W. Lugra, "Heavy Mineral Distribution Patterns And Characteristics Of Sea Floor Surficial Sediment At East Bali Waters, Bali Province," *Bulletin Of The Marine Geology*, vol. 26, 2011.
[13] J. Best, "Human, environmental costs of sand, gravel mining overlooked — study," Education News Asia Canada Europe, 2021. [Online]. Available: https://www.mining.com/human-environmental-costs-of-sand-gravel-mining-overlooked-study/.
[14] M. M. Ba-Abbad, A. Benamour, D. Ewis, A. W. Mohammad, and E. Mahmoudi, "Synthesis of Fe3O4 Nanoparticles with Different Shapes Through a Co-Precipitation Method and Their Application," *Jom,* vol. 74, no. 9, pp. 3531-3539, 2022, doi: 10.1007/s11837-022-05380-3.
[15] I. A. Tyurikova, S. E. Alexandrov, K. S. Tyurikov, D. A. Kirilenko, A. B. Speshilova, and A. L. Shakhmin, "Fast and Controllable Synthesis of Core-Shell Fe(3)O(4)-C Nanoparticles by Aerosol CVD," *ACS Omega,* vol. 5, no. 14, pp. 8146-8150, Apr 14 2020, doi: 10.1021/acsomega.0c00392.
[16] Z. I. Takai, Mustafa, M. K., Asman, S., & Sekak, K. A., "Preparation and Characterization of Magnetite (Fe3O4) nanoparticles By SolGel Method," *International Journal of Nanoelectronics and Materials,* vol. 12, pp. 37-46, 2019. [Online]. Available: https://www.researchgate.net/publication/330511880.
[17] S. S. A. Erwin , P. Adhy, N. Utari , W. Ayu , Y. Wita, & S. Nani "Magnetic iron oxide particles (Fe3O4) fabricated by ball milling for improving the environmental quality," *IOP Conf. Ser.: Mater. Sci. Eng.*, 2020, doi: 10.1088/1757-899X/845/1/012051.

[18] E. A. Bakr, M. N. El-Nahass, W. M. Hamada, and T. A. Fayed, "Facile synthesis of superparamagnetic Fe(3)O(4)@noble metal core-shell nanoparticles by thermal decomposition and hydrothermal methods: comparative study and catalytic applications," *RSC Adv,* vol. 11, no. 2, pp. 781-797, Dec 24 2020, doi: 10.1039/d0ra08230a.
[19] Darminto et al., "Preparing Fe[sub 3]O[sub 4] Nanoparticles from Fe[sup 2+] Ions Source by Co-precipitation Process in Various pH," *presented at the AIP Conference Proceedings*, 2011.
[20] M. S. Yusuf, S. S, and R. Rahmasari, "Synthesis Processing Condition Optimization of Citrate Stabilized Superparamagnetic Iron Oxide Nanoparticles using Direct Co-Precipitation Method," *Biomedical and Pharmacology Journal,* vol. 14, no. 3, pp. 1533-1542, 2021, doi: 10.13005/bpj/2255.
[21] M. Rahmayanti, "Synthesis of Magnetite Nanoparticles Using The Reverse Co-precipitation Method With NH4OH as Precipitating Agent and Its Stability Test at Various pH," *Natural Science: Journal of Science and Technology,* vol. 9, no. 3, pp. 54-58, 2020, doi: 10.22487/25411969.2020.v9.i3.15298.
[22] S. Nurjanah, "Sintesis Dan Karakterisasi Nanopartikel Magnetik Fe_3O_4 Pasir Besi Glagah Kulon Progo Dengan Metode Kopresipitasi," *UNY Journal*, 2018. [Online]. Available: http://eprints.uny.ac.id/id/eprint/57966.
[23] L. B. H. Rahayu, Wulandari, I. O., Santjojo, D. H., Sabarudin, A., "Pengaruh Kecepatan Pengadukan terhadap Karakteristik Nanopartikel Fe3O4 dengan Pelapisan Permukaan berbasis Polivinil Alkohol dan Glutaraldehid sebagai agen Crosslinker," *Natural B,* vol. 4, 2018.
[24] M. S. Adhim, "Synthesis Of Fe_3O_4 (Magnetite) Nanoparticles From Iron Stone Using Co-Precipitation Method With Ph Variation," *ITS Repository*, vol. Bachelor, 2018.
[25] D. Kiani, "X-Ray Diffraction (XRD)," in *Springer Handbook of Advanced Catalyst Characterization*, I. E. Wachs and M. A. Bañares Eds. Cham: Springer International Publishing, 2023, pp. 519-539.
[26] J. Madhavi, "Comparison of average crystallite size by X-ray peak broadening and Williamson–Hall and size–strain plots for VO2+ doped ZnS/CdS composite nanopowder," *SN Applied Sciences,* vol. 1, no. 11, p. 1509, 2019/10/29 2019, doi: 10.1007/s42452-019-1291-9.
[27] M. Lee, *X-RAY Diffraction for Materials Research From Fundamentals to Applications*. Apple Academic Press, Inc., 2016.
[28 J. M. e. al., "University of Wisconsin, Madison ChemPRIME," libretexts, 2023. [Online]. Available: https://LibreTexts.org. [29] M. Sinhababu *et al.*, "Surface Treatment of Industrial-Grade Magnetite Particles for Enhanced Thermal Stability and Mitigating Paint Contaminants," *Nanomaterials (Basel),* vol. 11, no. 9, Sep 4 2021, doi: 10.3390/nano11092299.
[30] L. Aspillaga, D. Jan Bautista, S. N. Daluz, K. Hernandez, J. A. Renta, and E. C. R. Lopez, "Nucleation and Crystal Growth: Recent Advances and Future Trends," *Engineering Proceedings,* vol. 56, no. 1, p. 22, 2023. [Online]. Available: https://www.mdpi.com/2673-4591/56/1/22.
[31] P. G. Vekilov, "Nucleation," *Cryst Growth Des,* vol. 10, no. 12, pp. 5007-5019, Nov 15 2010, doi: 10.1021/cg1011633.
[32] M. Rukhsar, Z. Ahmad, A. Rauf, H. Zeb, M. Ur-Rehman, and H. A. Hemeg, "An Overview of Iron Oxide (Fe3O4) Nanoparticles: From Synthetic Strategies, Characterization to

Antibacterial and Anticancer Applications," *Crystals,* vol. 12, no. 12, 2022, doi: 10.3390/cryst12121809.

[33] A. W. Y. Putra Parmita *et al.*, "Studi Pengaruh Temperatur Kalsinasi dalam Pembentukan Nanomagnetite dengan Metode Green Synthesis Ekstrak Daun Nanas," *SPECTA Journal of Technology,* vol. 7, no. 2, pp. 584-592, 2023, doi: 10.35718/specta.v7i2.940.

[34] Resetiana Dwi Desiatia, Eni Sugiartia, Safitry Ramandhany, "Analisa Ukuran Partikel Serbuk Komposit NiCrAl dengan Penambahan Reaktif Elemen untuk Aplikasi LAPISAN Tahan Panas," *METALURGI,* vol. 1, pp. 27 - 34, 2018.

[35] A. Sirivat and N. Paradee, "Facile synthesis of gelatin-coated Fe3O4 nanoparticle: Effect of pH in single-step co-precipitation for cancer drug loading," *Materials & Design,* vol. 181, 2019, doi: 10.1016/j.matdes.2019.107942.

[36] F. J. Link and J. Y. Y. Heng, "Unraveling the Impact of pH on the Crystallization of Pharmaceutical Proteins: A Case Study of Human Insulin," *Cryst Growth Des,* vol. 22, no. 5, pp. 3024-3033, May 4 2022, doi: 10.1021/acs.cgd.1c01463.

[37] K. C. Chinnam, "Capacitive pH-Sensors using pH sensitive polymer," IMEGO: Applied Micro Sensor Systems, p. 56, 2009. [Online]. Available: http://www.ep.liu.se.

[38] I. K. U. HASANAH, "*Sintesis Nanopartikel Maghemit (Γ-Fe_2O_3) Sebagai Pigmen Dari Limbah Besi Bubut Dengan Variasi Prekursor Menggunakan Metode Presipitasi – Kalsinasi*," Etheses of Maulana Malik Ibrahim State Islamic University, 2019.

[39] S. Nelms. "How to Improve Your ICP-MS Analysis, Part 1 Contamination." https://www.thermofisher.com/blog/analyteguru/How-to-Improve-Your-ICP-MS-Analysis-Part-1-Contamination.